ADVANCED MATERIALS
www.advmat.de

Predesign of Covalent-Organic Frameworks for Efficient Photocatalytic Dehydrogenative Cross-Coupling Reaction

Yu Chen, Sheng-Nan Sun, Xiao-Hong Chen, Ming-Lin Chen, Jiao-Min Lin, Qian Niu, Shun-Li Li, Jiang Liu,* and Ya-Qian Lan**

The dehydrogenative cross-coupling reaction is the premier route for synthesizing important 4-quinazolinone drugs. However, it usually requires high reaction temperature and long reaction time, and the yield of the final product is low. Here two stable and photosensitive covalent-organic frameworks (COFs), TAPP-An and TAPP-Cu-An are purposefully designed and constructed to serve as unprecedented heterogeneous tandem catalysts to complete dehydrogenative cross-coupling reactions in a short time and under mild reaction conditions (room temperature and light), leading to the high-efficient photosynthesis of 4-quinazolinones. Particularly, TAPP-Cu-An is the best heterogeneous catalyst currently available for the synthesis of 4-quinazolinones, even surpassing all the catalysts reported so far. It also enables one-step photosynthesis of 4-quinazolinones with higher conversion (>99%) and selectivity (>99%) in a shorter time, and the product can be easily prepared on a gram scale. Extensive experiments combined with theoretical calculations show that the excellent photogenerated charge separation and transport capability, as well as the synergistic An-Cu catalysis in TAPP-Cu-An are the main driving forces for this efficient reaction.

1. Introduction

Quinazolinones represent a class of drug molecules with excellent physiological and pharmacological activities, which have been widely used in medicine and pesticide fields.[1,2] In general, these compounds are obtained by dehydrogenative cross-coupling reaction,[3,4] alkenes difunctionalization reaction,[5,6] oxidative ring-opening reaction,[7,8] and cycloaddition reaction.[9,10] Especially, dehydrogenative cross-coupling reaction, an important method to construct C—C, C—N, and C—O bonds, can achieve the synthesis of complex polycyclic structures under relatively mild conditions.[11] Therefore, widespread attention has been paid to synthesizing 4-quinazolinone via inter- and intramolecular dehydrogenative cross-coupling of cycloamine and 2-aminobenzaldehyde (alcohol).[12] However, there are still some drawbacks to this method, for example, complex reaction conditions, high energy consumption (high temperature and long reaction time), and low yield of product. Moreover, the common use of homogeneous catalysts (Cu salt or small organic molecules) makes recycling hard.[13] In this case, it is very important and necessary to develop effective heterogeneous catalysts to realize the synthesis of 4-quinazolinone with high selectivity and conversion by the dehydrogenative cross-coupling reaction under milder reaction conditions with lower energy consumption and shorter time, for example, photocatalysis.

In order to achieve the above purpose, it is crucial to systematically study the different catalytic processes involved in the dehydrogenative cross-coupling reaction for the synthesis of 4-quinazolinone.[14] This reaction usually undergoes successive dehydrogenative oxidation of cycloamines to imine, nucleophilic addition (a spontaneous process), and intramolecular cross-oxidative coupling between 2-aminobenzaldehyde (alcohol) and imine under O_2 atmosphere, which acts as an oxidizing agent to activate the key reactants. Therefore, we believe that as far as the structural design of the catalyst is concerned, the corresponding effective catalyst should have the following characteristics: i) High structural stability to achieve heterogeneous catalysis. ii) Responding to specific external stimuli (e.g., sunlight) so that the reaction occurs under mild and low energy conditions. iii) The ability to activate O_2 and complete the subsequent oxidation reaction processes. iv) Active Cu sites to catalyze intramolecular cross-oxidative coupling processes. If these advantages are combined into a catalyst, it is possible to achieve the synthesis of

Y. Chen, S.-N. Sun, X.-H. Chen, M.-L. Chen, J.-M. Lin, S.-L. Li, J. Liu, Y.-Q. Lan
National and Local Joint Engineering Research Center of MPTES in High Energy and Safety LIBs
Engineering Research Center of MTEES (Ministry of Education), and Key Lab. of ETESPG (GHEI)
School of Chemistry
South China Normal University
Guangzhou 510006, China
E-mail: linjm@m.scnu.edu.cn; liuj0828@m.scnu.edu.cn; yqlan@njnu.edu.cn, yqlan@m.scnu.edu.cn

Q. Niu
Jiangsu Collaborative Innovation Centre of Biomedical Functional Materials
School of Chemistry and Materials Science
Nanjing Normal University
Nanjing 210023, China

The ORCID identification number(s) for the author(s) of this article can be found under https://doi.org/10.1002/adma.202413638

DOI: 10.1002/adma.202413638

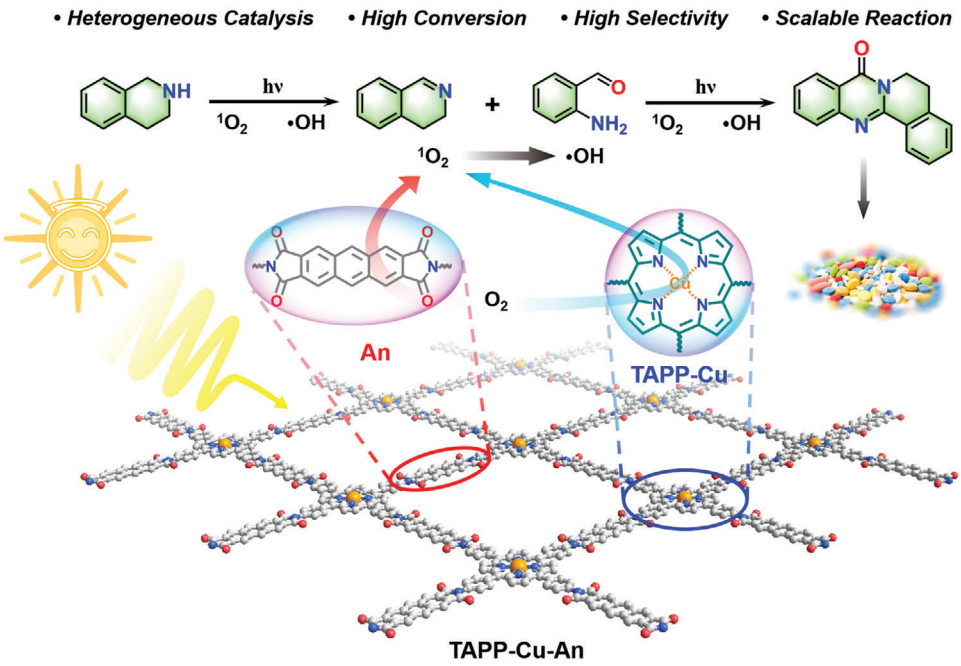

Scheme 1. Synthesis of 4-quinazolinone drug molecules through efficiently photocatalytic dehydrogenative cross-coupling reaction by photosensitive and stable porphyrin-based COF.

4-quinazolinone in a more efficient manner. With regard to these design requirements for catalysts, covalent-organic frameworks (COFs), a new class of crystalline porous material, may be an ideal catalyst model to study this reaction since their structures can be controlled by pre-design.[15–17] And with their high stability and structural designability, they have been widely applied in gas storage and separation,[18–20] photo-electrocatalysis,[21–23] batteries, and energy storage.[24–26] It is worth noting that some works have been done on the application of COF materials in organic catalysis.[27–35]

Based on the above considerations, we designed and synthesized a series of COF tandem catalysts, **TAPP-An** and **TAPP-M-An** (M = Mn, Cu), using porphyrins/metalloporphyrins (TAPP/TAPP-M) and anthracene anhydride (An). These catalysts exhibit very high structural stability and excellent light capture capability. The light absorption range covers the entire ultraviolet to infrared region. Significantly, both anthracene and metalloporphyrin monomers have the ability to efficiently absorb sunlight and activate O_2 to $^1O_2$.[42,43] Besides, the metalloporphyrin can also serve as an active component to catalyze the intramolecular cross-oxidation coupling reaction. It is clear that the advantages of these COF materials are well suited to the design requirements of the catalysts to achieve more advanced dehydrogenative cross-coupling reactions. Thus, the above COF materials were used as photocatalysts to catalyze a light-driven dehydrogenative cross-coupling reaction to synthesize 4-quinazolinone derivatives with 1,2,3,4-tetrahydroisoquinoline and 2-aminobenzaldehyde as reactants and without the addition of any other reagents. Systematic catalytic studies revealed that **TAPP-An** can effectively complete the photo-induced dehydrogenation of 1,2,3,4-tetrahydroisoquinoline to 3, 4-dihydroisoquinoline, while **TAPP-M-An** can effectively complete the cross-oxidative coupling reaction of 3, 4-dihydroisoquinoline and 2-aminobenzaldehyde to produce 5, 6-dihydro-8*H*-isoquinolino[1, 2-*b*]quinazolin-8-one (3a). Moreover, when **TAPP-Cu-An** was used as a heterogeneous catalyst, the one-step photocatalytic conversion of 1,2,3,4-tetrahydroisoquinoline and 2-aminobenzaldehyde to 3a can be realized in a short reaction time (6 h) with conversion and selectivity up to 99% (**Scheme 1**). More importantly, the reaction also allows for gram-scale preparation of 3a in such a mild and low-energy manner. This work confirms for the first time the important application of crystalline COF tandem catalyst in the synthesis of 4-quinazolinone compounds.

2. Results

2.1. Synthesis and Characterization of Covalent-Organic Frameworks photocatalysts

Precursor 5, 10, 15, 20-Tetrakis(4-aminophenyl) porphyrin (denoted TAPP) was obtained from commercial sources, and other two precursors 1H, 3H-Anthra[2, 3-c:6, 7-c']difuran-1, 3, 7, 9-tetrone (denoted An) and 5, 10, 15, 20-Tetrakis(4-aminophenyl) porphyrin-M (M = Mn, Cu, denoted TAPP-M) were prepared according to the previously reported methods.[36,37] **TAPP-An** and **TAPP-M-An** were synthesized using an ionothermal solvent-free method in a eutectic salt mixture of anhydrous zinc chloride ($ZnCl_2$) and sodium chloride (NaCl) under vacuum conditions (**Figure 1a**) (see SI).[38] Powder X-ray diffraction (PXRD) patterns of **TAPP-An** and **TAPP-M-An** revealed that they are isostructural. Thus, **TAPP-An** was taken as an example for the structural analysis (the structural analysis for **TAPP-M-An** (M = Mn, Cu) was provided in Figure S2, Supporting Information). As shown in Figure 1b, the PXRD pattern of **TAPP-An** displayed a strong

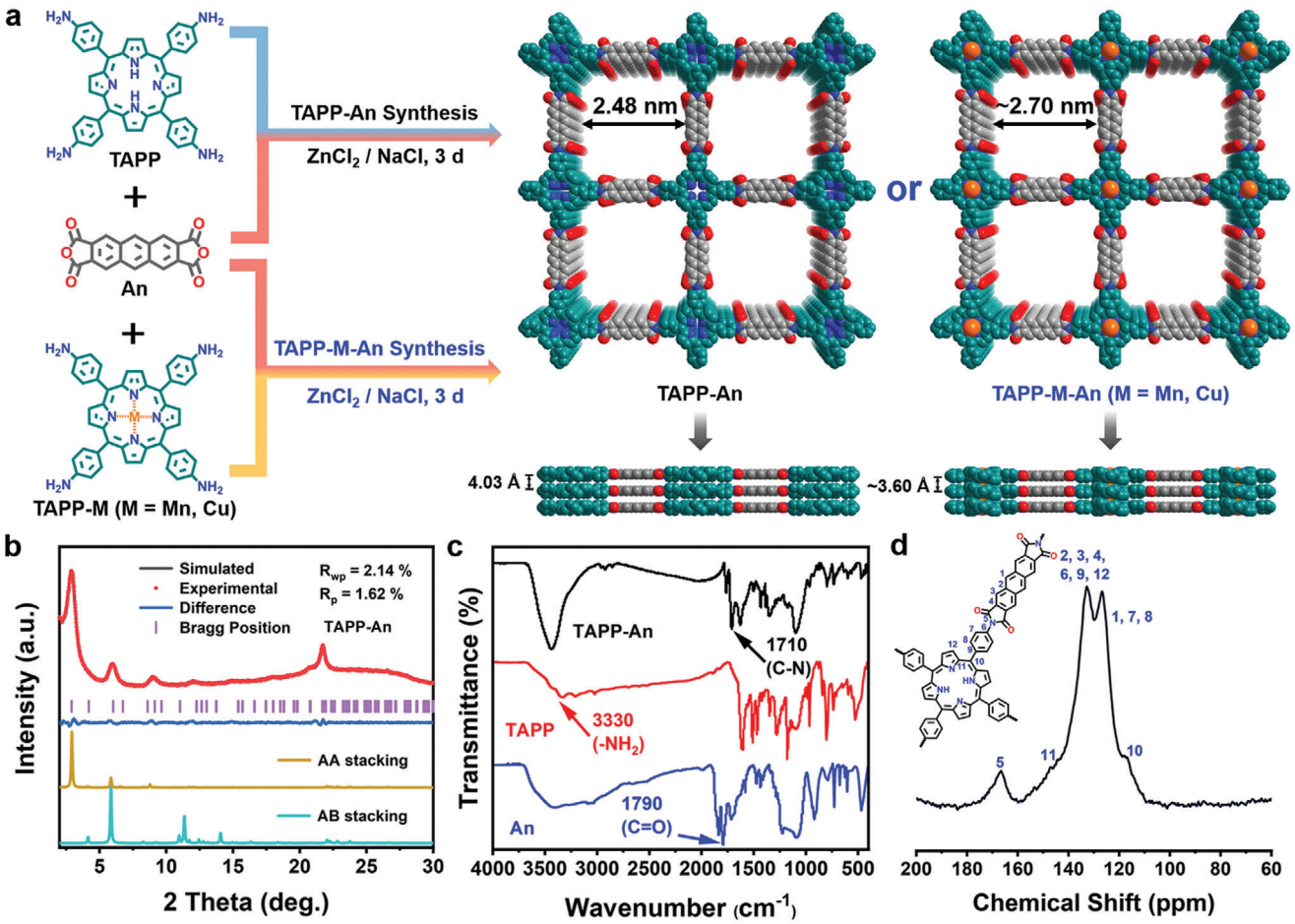

Figure 1. a) Schematic of the synthesis of **TAPP-An** and **TAPP-M-An**. b) Experimental and simulated PXRD patterns of **TAPP-An**. c) FT-IR spectra of **TAPP-An**. d) ^{13}C CP/MAS NMR spectrum of **TAPP-An**. (The assignments of ^{13}C chemical shifts of **TAPP-An** are indicated in the chemical structure.).

diffraction peak at $2\theta = 2.9°$, along with several minor peaks at 6.0°, 9.1°, 12.3° and 21.7°. To elucidate its crystal structure, two possible 2D layer stacking models (AA and AB stacking models) that may crystalize in the *P*-42*m* and *P*-421*m* space groups were built up using Materials Studio. The results revealed that the experimental PXRD pattern matches well with the simulated one from the AA stacking model. To further confirm this structural model, structural refinement based on the perimental PXRD data of **TAPP-An** was carried out. The unit cell parameters of $a = b = 30.19$ Å, $c = 4.03$ Å with good residual factors of $R_{wp} = 2.14\%$ and $R_p = 1.62\%$ can be achieved using Pawley refinement, demonstrating the validity of this calculation model (the structural information for the AB stacking model was displayed in Figure S6, Supporting Information). According to this structural model, the PXRD peaks at $2\theta = 2.9°$, 6.0°, 9.1°, 12.3°, and 21.7° can be attributed to the (110), (200), (300), (400), and (700) crystal planes, respectively (Figure 1b). After AA stacking, **TAPP-An** has a large square channel (theoretical pore size, 2.48 × 2.48 nm) along the *c*-axis and the interlayer distance is 4.03 Å (Figure 1a). In the Fourier transform infrared (FT-IR) spectroscopy of **TAPP-An**, the tensile vibration peak a≈3330 cm^{-1} for the NH_2- groups disappeared, while the tensile vibration peak at 1790 cm^{-1} for C=O bonds remained, and a new characteristic peak at 1710 cm^{-1} that corresponding to the C-N stretching vibration of amides is appeared. These suggest the occurrence of the condensation reaction between the TAPP and An units, and the formation of the amide connection network (Figure 1c). In addition, in the ^{13}C CP/MAS NMR spectrum of **TAPP-An**, the signals of the main carbon atoms and the carbon atom involved in the amide bond (at 166 ppm) can all be observed (Figure 1d), further verifying the successful synthesis of this compound.

Nadsorption-desorption measurements at 77 K revealed that the Brunauer-Emmett-Teller (BET) surface area of **TAPP-An** is ≈458.3 m^2 g^{-1} and the pore size is ≈2.50 nm, which is in good agreement with the results predicted from the theoretical structure model (**Figure 2a**). Scanning electron microscopy (SEM), transmission electron microscopy (TEM), and high-resolution TEM (HR-TEM) were conducted to characterize the morphology of **TAPP-An**, which revealed that it is rough spherical nanoparticles (domain size in the range of > 300 nm) (Figures S26–S28, Supporting Information). In the HR-TEM images, a lattice spacing of 3.48 Å can be observed, which corresponds to the (331) crystal face of **TAPP-An** (Figure S26b, Supporting Information), validating the high crystallinity of this compound. Besides, the energy dispersive X-ray spectroscopy (EDS) mapping shows that the C, N, and O elements are evenly distributed across

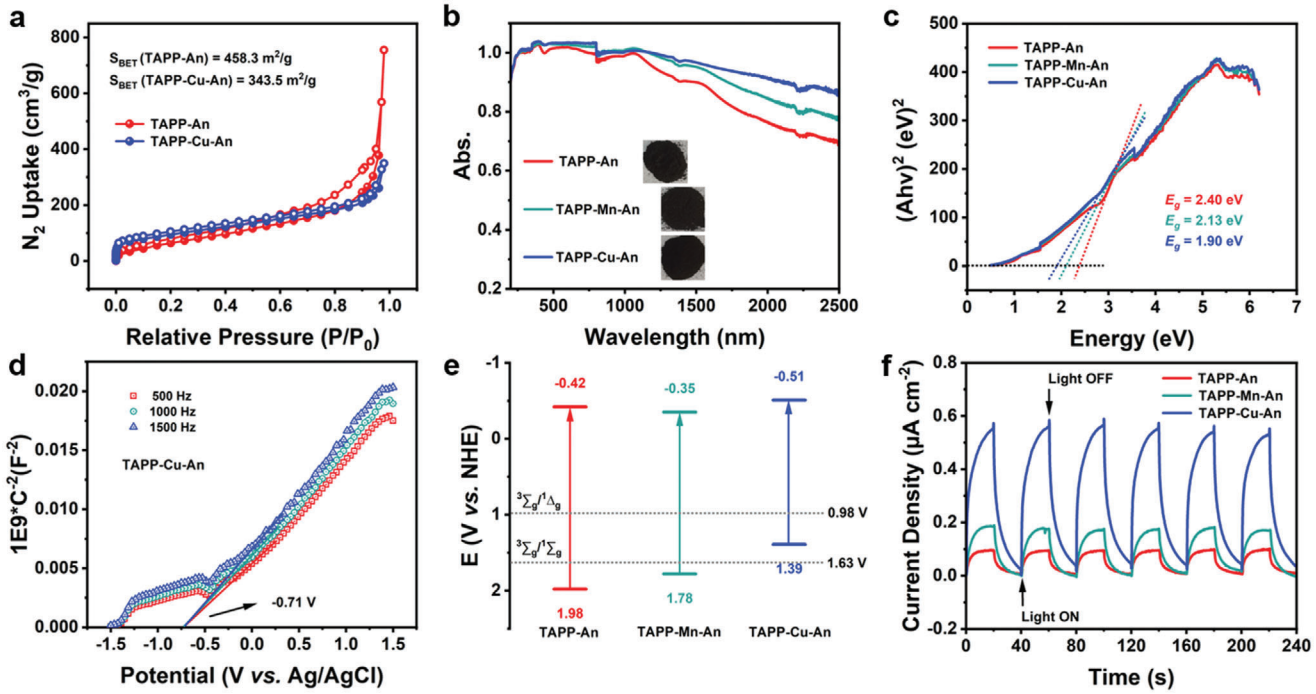

Figure 2. a) N_2 adsorption curve of **TAPP-An**, **TAPP-Cu-An** at 77 K. b) Solid-state UV/Vis absorption spectra of **TAPP-An**, **TAPP-M-An** (M = Mn, Cu). c) Tauc plots of **TAPP-An**, **TAPP-M-An** (M = Mn, Cu) calculated by the Kubelka–Munk (KM) method. d) Mott–Schottky plot for **TAPP-Cu-An**. e) Band-structure diagram of **TAPP-An**, **TAPP-M-An** (M = Mn, Cu). f) Transient photocurrent response of **TAPP-An**, **TAPP-M-An** (M = Mn, Cu).

the nanoparticles, indicating the high uniformity of **TAPP-An** (Figure S26c, Supporting Information). ICP results showed that the content of residual Zn in all COFS was negligible (Table S4, Supporting Information). In order to investigate whether these COFs can remain stable in the dehydrogenative cross-coupling reaction conditions, their thermal and chemical stability were measured. The thermogravimetric analysis (TGA) of **TAPP-An** shows that there is no significant weightlessness before 400 °C, suggesting good thermal stability (Figure S13, Supporting Information). In addition, when the samples of **TAPP-An** were immersed in different organic solvents or an aqueous solution with different pH values for one weak, their PXRD pattern matched well with the simulated one, indicating the structural skeleton of **TAPP-An** remained intact, and further proved that **TAPP-An** had high chemical stability (Figure S29, Supporting Information). Similarly, the structure and morphology of **TAPP-M-An** (M = Mn, Cu) were well characterized by PXRD, FI-IR, ^{13}C CP/MAS NMR, TGA, N_2 adsorption, SEM, TEM, EDS mapping and XPS(Figures S2–S28, S30, S50, Supporting Information).

2.2. Photophysical Characterization of TAPP-An and TAPP-M-An (M = Mn, Cu)

According to the design requirements of an ideal photocatalyst for the dehydrogenative cross-coupling reaction to synthesize 4-quinazolinone, its photophysical properties play an important role in this reaction. Thus, we investigated the photophysical properties of these COF materials first. The UV–vis diffuse reflection spectroscopy (DRS) measurements reveal that these COFs display exceptional light absorption within the wavelength range of 200–2500 nm, suggesting their light absorption range can cover the entire ultraviolet to infrared region, which is rarely observed among COF materials (Figure 2b). The optical band gaps of **TAPP-An** and **TAPP-M-An** (M = Mn, Cu) were determined by Tauc diagram analysis using Kubelka–Munk (KM) method, and the results reveal that they are 2.40, 2.13, and 1.90 eV, respectively (Figure 2c). In addition, Mott-Schottky (MS) measurements were conducted to determine the conduction band (CB) positions of **TAPP-An** and **TAPP-M-An** (M = Mn, Cu) (Figure 2d and Figures S31, S32, Supporting Information), which were −0.42, −0.35, and−0.51 V, respectively. Thus, their valence band (VB) were estimated to be 1.98, 1.78, and 1.39 V, respectively (Figure 2e), which are similar to those obtained from the UV photoelectron spectroscopy (UPS) measurements (2.05, 1.83, and 1.38 V, respectively, Figures S33–S35, Supporting Information).[39] Subsequently, the photocurrent response measurements were conducted to characterize the separating efficiency of light-generated carriers. The results reveal that **TAPP-Cu-An** has the highest transient photocurrent response, indicating its superior charge separation performance, as compared to the other two samples (Figure 2f).

2.3. Photocatalytic Dehydrogenative Cross-Coupling Reaction

Based on the excellent photophysical properties and high stability of **TAPP-An** and **TAPP-M-An** (M = Mn, Cu), and considering the existing problems of the synthesis of 4-quinazolinone, we used these COFs as catalysts for the photosynthesis

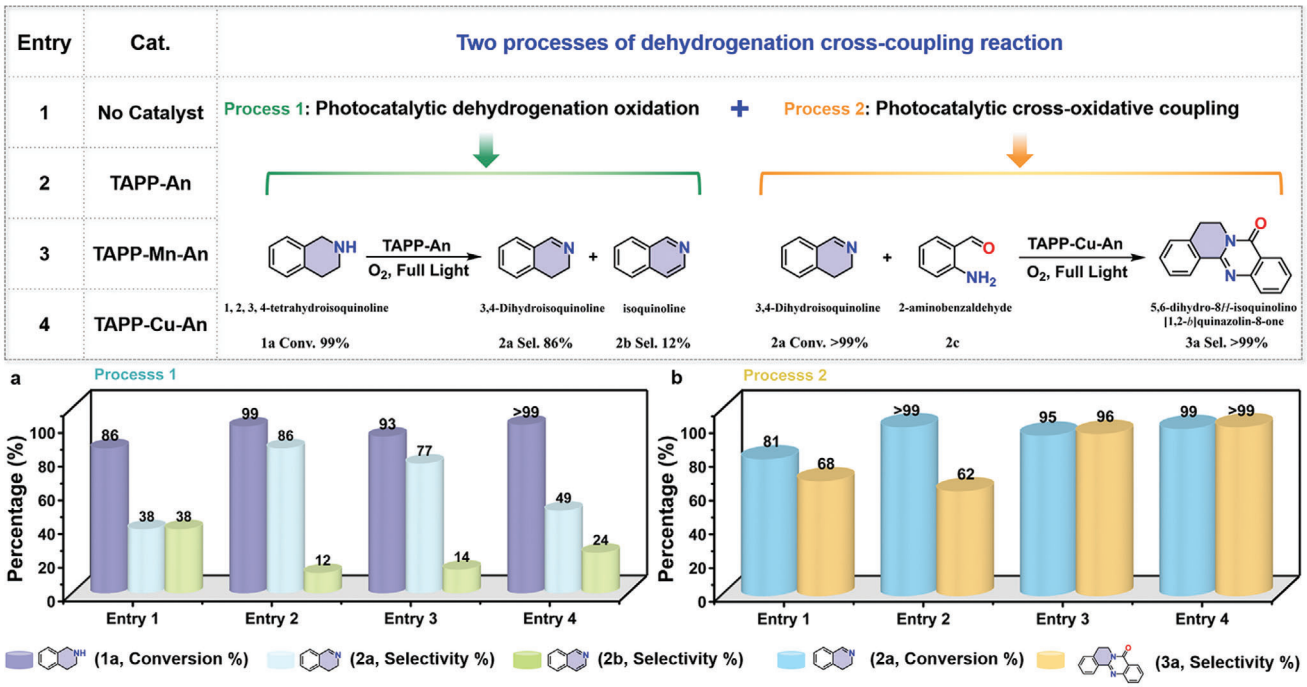

Figure 3. a) Conversion and selectivity of Process 1 over four different catalyst groups (No Catalyst, **TAPP-An**, **TAPP-M-An** (M = Mn, Cu)). b) Conversion and selectivity of Process 2 over four different catalyst groups (No Catalyst, **TAPP-An**, **TAPP-M-An** (M = Mn, Cu)). (Conversion and selectivity were quantitatively calculated by GC-MS.).

of 4-quinazolinone, with 5,6-dihydro-8H-isoquinolino[1,2-b]quinazolin-8-one (3a) as a model product. According to the existing reaction mechanism, there are two separate processes in the synthesis of 3a, that is, the dehydrogenative oxidation process of 1,2,3,4-tetrahydroisoquinolines (1a), and the intramolecular oxidative coupling process after the addition of dehydrogenative oxidation products to amino groups. In order to evaluate whether these COF catalysts can achieve the synthesis of 3a and to determine the reaction mechanism, we studied the two reaction processes step by step.

First, we investigated the photocatalytic performance of **TAPP-An** and **TAPP-M-An** (M = Mn, Cu) for the dehydrogenative oxidation of 1a to form the target product 3, 4-dihydroisoquinoline (2a). The liquid products were analyzed by gas chromatography-mass spectrometry (GC-MS). As shown in **Figure** 3a, for these three COF photocatalysts, **TAPP-An** shows the best photocatalytic performance with the substrate conversion of more than 99%, and selectivity of the products 3, 4-dihydroisoquinoline (2a) and isoquinoline (2b) reaches 86% and 12%, respectively. Compared with those without catalysts, **TAPP-An** could effectively increase the 2a selectivity and reduce the generation of by-product 2b. Besides, a series of controlled experiments were conducted to determine the indispensable reaction conditions (Table S5, Supporting Information). First, the photocatalytic performance of the TAPP and An monomers were examined. The results reveal that both monomers can achieve a good substrate conversion of 88% (for TAPP, homogeneous catalyst) and 96% (for An), but the product selectivity is quite different. Specifically, the selectivity of the product 2a of TAPP (Sel. 2a, 9%; 2b, 25%) is much lower than that of An (Sel. 2a, 51%; 2b, 32%), which suggests that in **TAPP-An**, An plays the major role in determining the selectivity of 2a product. Specifically, the selectivity of the product 2a of TAPP (Sel. 2a, 9%; 2b, 25%) is much lower than that of An (Sel. 2a, 51%; 2b, 32%), which suggests that in **TAPP-An**, An can improve the selectivity of 2a product. In addition, photocatalyst, oxygen, and light are all essential conditions for this dehydrogenative oxidation reaction. Without these conditions, only a little or trace 2a product can be observed. Totally, under the O_2 atmosphere, **TAPP-An** can convert 1a to 2a with high conversion (99%) and high selectivity (86%) upon 12 h light-irradiation, which are better than those of **TAPP-M-An**. These results suggest in this step of the reaction, the An unit can improve the selectivity of 2a product, while the TAPP-M unit may lead to over oxidate 1a into 2b product. Thus, **TAPP-An** can indeed be an effective photocatalyst for this dehydrogenative oxidation reaction, in which An unit can achieve regulation of the product selectivity.

Subsequently, these COFs were further applied to study the photocatalytic intramolecular oxidative coupling reaction, which occurs after the nucleophilic addition of 2a and 2- aminobenzaldehyde (2c). As displayed in Figure 3b, for this photocatalytic cross-coupling reaction, **TAPP-Cu-An** shows the best photocatalytic performance, with the 2a conversion of 99% and 3a selectivity of >99%, which is slightly higher than that of **TAPP-Mn-An** (Conv. 95% and Sel. 96%). Moreover, although **TAPP-An** can achieve high conversion (>99%) of 2a, it is hard to obtain the target product (3a) with high selectivity (62%). These results demonstrate the importance of the metal catalytic site (Cu^{2+}, Mn^{2+}) in this step of the reaction (Cu is the best), which is consistent with the previous report.[13] To further investigate the catalytic site, the photo-catalytic performances of the two monomers (TAPP-Cu (homogeneous) and An) were measured, and a series of controlled experiments were conducted. As shown in Table S6

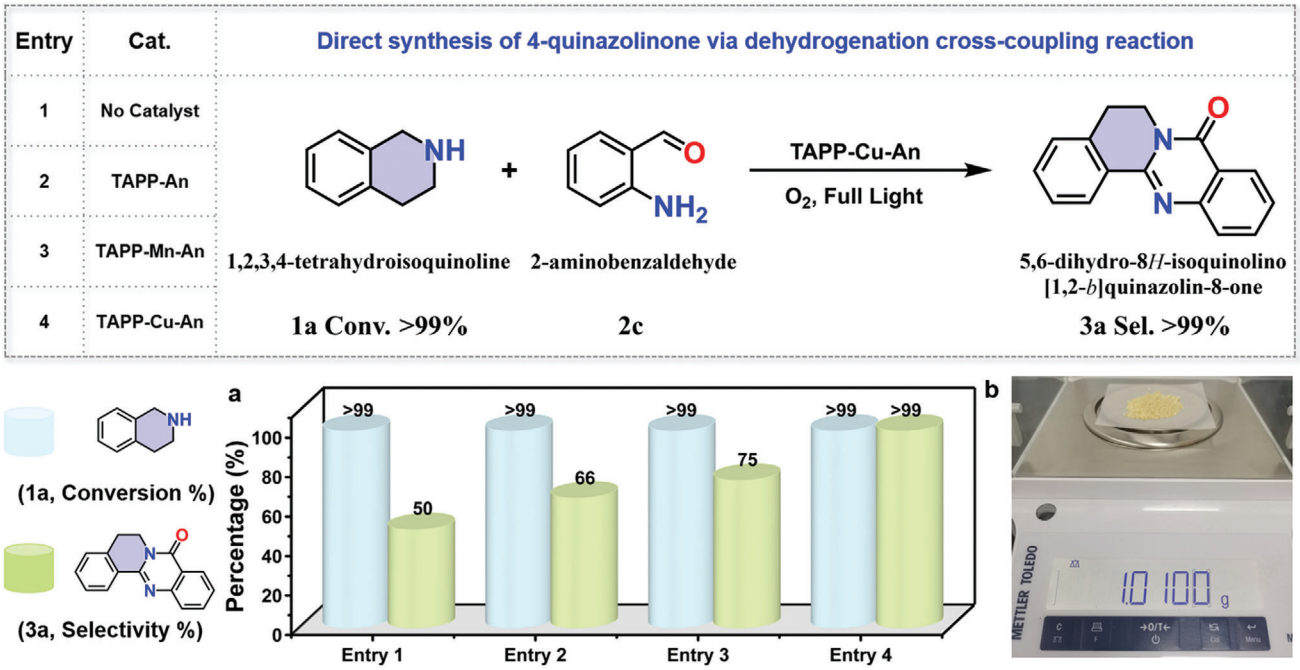

Figure 4. a) Conversion and selectivity of dehydrogenative cross-coupling reaction over four different catalyst groups (No Catalyst, **TAPP-An**, **TAPP-M-An** (M = Mn, Cu)). b) The product yield of the gram-scale reaction. (Conversion and selectivity were quantitatively calculated by GC-MS.).

(Supporting Information), the conversion of 2a catalyzed by TAPP-Cu and An are >99% and 93%, and the 3a product selectivity are 95% and >99%, respectively. It can be clearly seen that the photocatalytic performance of TAPP-Cu is slightly better than that of An, which further proves that although both TAPP-Cu and An contribute to this reaction process, the TAPP-Cu plays the major catalytic role. In Ar atmospheres, the photocatalytic performance decreases significantly, proving O_2 is involved in this reaction. Under visible light and dark environments, the photocatalytic performance decreases dramatically, indicating that this reaction requires light excitation and different light bands have a great influence on it. Totally, under an O_2 atmosphere, **TAPP-Cu-An** can convert 2a to 3a with a high conversion of 99% and high selectivity of >99% through photocatalysis within 6 h. Therefore, **TAPP-Cu-An** is an effective photocatalyst for the oxidative coupling reaction between 2a and 2c, in which TAPP-Cu is the specific catalytic site.

The above experiments evident that the An unit in the COFs can improve the 2a product selectivity in the first step of the reaction (dehydrogenative oxidation of cycloamines), while the TAPP-Cu unit can improve the yield of 3a product in the second step of the reaction (intramolecular oxidative cross-coupling following nucleophilic addition of amino to cycloamines). Based on this fact, we further verified whether **TAPP-Cu-An** can be a tandem photocatalyst to directly complete the dehydrogenative cross-coupling between 1a and 2c. As shown in **Figure** 4a, **TAPP-Cu-An** exhibits the best catalytic performance, and it can achieve both substrate conversion and product selectivity up to 99% within 6 h. For **TAPP-Mn-An** and **TAPP-An**, although they can also achieve near 100% substrate (2a) conversion, the selectivity of 3a is only 66% and 75%, respectively. Similarly, for the control group without COF catalyst, although high substrate conversion (2a Conv. >99%) could be achieved, the target product selectivity (3a Sel. 50%) is much lower than that of all COF catalysts, which proves that COF catalyst played a good catalytic role for this reaction and greatly improved the product selectivity (3a). To further study the two different processes of this reaction, the photocatalytic performances of the two crucial monomers TAPP-Cu (homogeneous) and An, and a series of controlled experiments were investigated (Table S7, Supporting Information). For TAPP-Cu and An, the 2a substrate conversion is near 100%, but the product (3a) selectivity is ≈80% and 75%, respectively, indicating that both of them have a catalytic contribution to this reaction, and they have synergistic catalytic effect when they form COFs. No target product (3a) was observed under Ar atmosphere, visible light, or dark conditions, further proving that O_2 and light irradiation are essential for this reaction. To ensure the accuracy of catalytic reaction data, we measured and calculated the apparent quantum yield (AQY) and the reaction rate of the tandem reaction under ultraviolet and visible light irradiation (Table S8, Supporting Information). The results revealed that under ultraviolet light (350 nm) irradiation, the AQY is 6.86×10^{-7} and the reaction rate is 0.017 mmol $g^{-1}h^{-1}$, while under visible light (450 nm) irradiation, the AQY is 3.07×10^{-7} and the reaction rate is 0.010 mmol g^{-1} h^{-1}.

Based on the above experiments, it can be seen that in the first reaction process, the photocatalytic performance of **TAPP-Cu-An** is not as good as that of **TAPP-An**, which is mainly because although both An and TAPP-Cu can activate O_2 to oxidize 1a, the oxidation selectivity of TAPP-Cu cannot achieve the same level of An. While when TAPP-Cu and An joined together, the oxidation of O_2 after photoactivation is overactive, making 1a over oxidation, and thus for **TAPP-Cu-An**, the selectivity of the target product (3a) is not very high. On the other hand, in the second process,

TAPP-Cu-An displayed better photocatalytic performance than that of **TAPP-An**, which is mainly because the presence of metal sites can catalyze the intramolecular oxidation cross-coupling reaction, and thus the target product can be obtained in high selectivity. Totally, in the one-step tandem photocatalytic dehydrogenative cross-coupling reaction of 1a and 2c, **TAPP-Cu-An** displayed the best catalytic performance among the three COF materials. This is should be because in this one-step tandem photocatalytic reaction, the An and TAPP-Cu components in **TAPP-Cu-An** can cooperate together to achieve efficient O_2 activation for oxidizing 1a to form 2a with high selectivity, and then 2a nucleophilic addition with 2c, and quickly underwent intramolecular oxidative cross-coupling reaction to form 3a under the catalysis of TAPP-Cu component.

Considering the good catalytic performance and easy preparation of **TAPP-Cu-An**, the one-step tandem reaction was enlarged by ≈50 times. The result revealed that the substrate1a can be completely converted into 3a with ≈100% selectivity within 24 h, and ≈1 g of 3a can be obtained at one time (Figure 4b), indicating the great application potential of this **TAPP-Cu-An** photocatalyst. In addition, after photocatalytic reaction, all COF materials remained solids, suggesting their heterogeneous catalytic nature. Furthermore, the XRD, IR, and XPS patterns of these samples after photocatalytic reaction remain similar to those before the catalytic reaction, proving the high structural stability of these COF catalysts (Figures S47–S52, Supporting Information). To verify the heterogeneous catalytic stability of **TAPP-Cu-An**, we conducted 1 h catalytic cycles and gram-scale reaction cycles. The results revealed that in the 1 h catalytic cycle, the substrate conversion and product selectivity did not show significantly reduction until the seventh cycle (Figure S45, supporting information). Besides, in gram-scale reaction cycles, **TAPP-Cu-An** was able to maintain high substrate conversion (>99%) and product selectivity (99%) within 3 cycles (Figure S46, supporting information). These results proved that **TAPP-Cu-An** has high heterogeneous catalytic stability. To verify the importance of An in the tandem reaction, COF-366 and COF-366-Cu were synthesized as comparison samples (Figure S42, Supporting Information). Catalytic performance results revealed that for COF-366, the 1a conversion and 3a product selectivity are 90% and 60%, respectively, which are lower than that of **TAPP-An** (Figure S43, Supporting Information). While for COF-366-Cu, the 1a conversion and 3a product selectivity are 86% and 59%, respectively, which are lower than that of **TAPP-Cu-An**. These results suggest that both **TAPP-An** and **TAPP-Cu-An** with An unit have better catalytic performance than COF-366 and COF-366-Cu, suggesting An unit is indeed needed for our catalysts.

To further demonstrate the catalytic universality of **TAPP-Cu-An** in the one-step photosynthesis of 4-quinazolinone compounds, substrate extension studies were performed. As shown in **Table 1**, different substrates in this one-step reaction can proceed smoothly and provide the desired product with moderate to high product yield (see 3b-3f). The substituent groups in the aromatic ring (2d-2f) had little effect on the formation of the product. In particular, the enhanced conjugation effect of the pyridine ring on the substrate 2f was beneficial to the product formation with high selectivity, while the electron-withdrawing substituents on the aromatic ring of the substrate (2d,2e) were not conducive to the product formation. Meanwhile, the presence of an electron-withdrawing substituent (1b,1c) on the cyclic amine caused much less product formation. This phenomenon is mainly attributed to the substitution affecting the nucleophilicity of the reactive arylamine and the electron density of the double bond of the cycloamine intermediate. That is, the more nucleophilic the -NH_2 is, the better for the formation of the product, and the lower the electron density of double bonds in dihydroisoquinoline intermediates, the more favorable for the formation the product.

2.4. DFT Calculations and Mechanism

To further elucidate the reaction mechanism of the dehydrogenative cross-coupling reaction, we conducted comparative experiments. First, a series of quenching experiments were employed to study and confirm the reaction mechanism for process 1 and processec 2. The results indicated the generation of $^1O_2$, •OH, e^-, and h^+ during process 1 and processec 2 (**Figure 5a** and Figures S40a,b,c, S41, Supporting Information). Additionally, we performed EPR spin-trapping experiments using TEMP as a trapping agent, which confirmed the generation of $^1O_2$ (Figure 5b and Figure S40d,e,f, Supporting Information). Moreover, fluorescence lifetime measurements indicated that all COF materials exhibited fluorescence lifetimes exceeding 5 ns, with **TAPP-Cu-An** having the longest fluorescence lifetime (Figure 5**c**). This confirms that these COFs have stable e^- and h^+ separation abilities, with **TAPP-Cu-An** showing the most stable e^- and h^+ separation.

To determine the specific reaction mechanism of the tandem reaction, we performed density functional theory calculations. A simplified model, consisting of a porphyrin unit and four acid anhydrides, was used in our calculations. The optimization of the model was conducted at the M06L level using Gaussian 16 code. Frontier orbital analysis revealed that the highest occupied molecular orbital (HOMO) was mainly located around TAPP, and the lowest unoccupied molecular orbital (LUMO) was primarily distributed near the anhydride (An) unit (Figure S53a, Supporting Information). The **TAPP-Cu-An** showed similar distributions of HOMO and LUMO (Figure 5d). This indicates that the HOMO-to-LUMO electronic transition would result in a fully charge-separated excited state, which could enhance the probability of triplet state formation. Additionally, since the photogenerated electrons were mainly localized on the An unit, it is suggested that the An could be an important reactive site. The electronic properties of **TAPP-Cu-An** and **TAPP-Mn-An** we calculated using PBE functional with VASP code. Calculation results demonstrated that the band gaps of **TAPP-Cu-An** and **TAPP-Mn-An** are 0.685 and 0.247 eV (Figures S55, S56, Supporting Information). Compared with the Figure 2e, the band gaps of COFs are underestimated significantly, which is consistent with the previous report.[40] However, the energy band variation trends of **TAPP-Mn-An** and **TAPP-Cu-An** are consistent with the calculated results.

In the first catalytic process, when using **TAPP-An** as the catalyst, the calculations showed that 1a could adsorb onto both An and TAPP with similar adsorption energies (Figure S53f, h, Supporting Information). However, when **TAPP-Cu-An** was used as the catalyst, the adsorption energy of 1a with TAPP-Cu was significantly higher than with An, potentially leading to over-oxidation of 1a (Figure S53b,d, Supporting Information). This suggests

Table 1. The universality study of photocatalytic dehydrogenative cross-coupling reaction over **TAPP-Cu-An**.

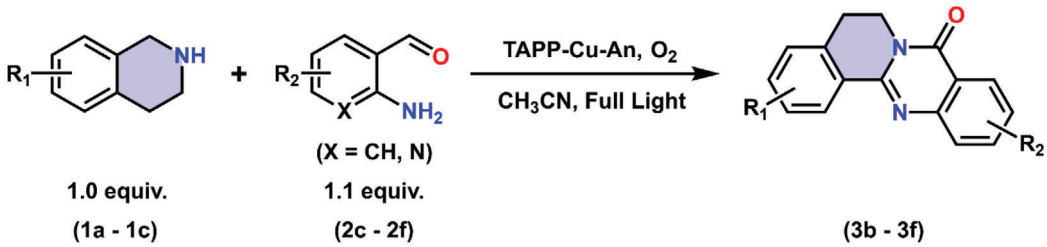

Entry[a]	Substrate 1	Substrate 2	Product	Yield (%)[b]
1	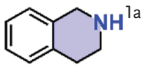 1a	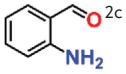 2c	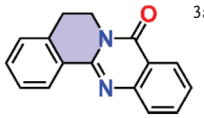 3a	>99
2	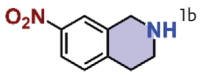 1b	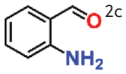 2c	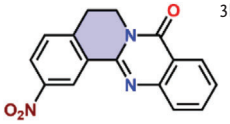 3b	75
3	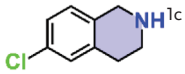 1c	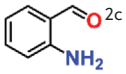 2c	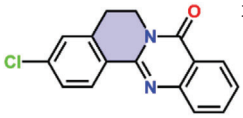 3c	57
4	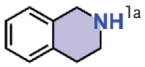 1a	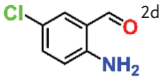 2d	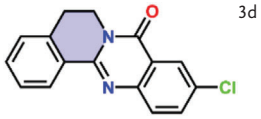 3d	68
5	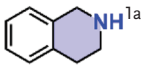 1a	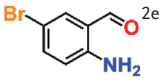 2e	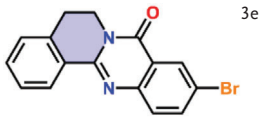 3e	60
6	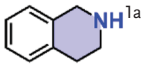 1a	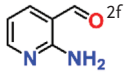 2f	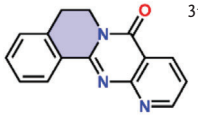 3f	84

[a] Reaction conditions: substrate (1:1.1 equiv.); **TAPP-Cu-An** 50 mg; CH_3CN 20 mL; bubbled with O_2 for 10 min, full light 12 h; [b] Yield of the isolated product.

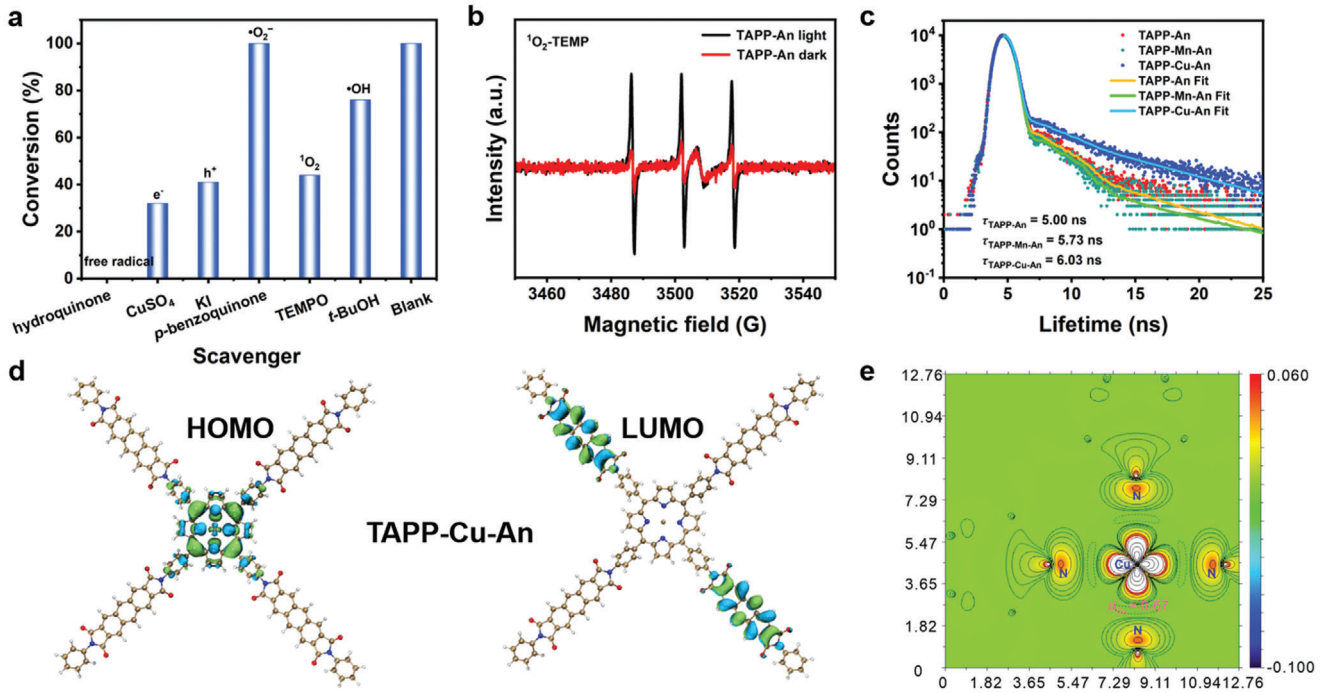

Figure 5. a) Radical quenching experiments for reaction process 1. b) $^1O_2$ radical trapping experiments for reaction process 1. c) Fluorescence lifetime of **TAPP-An**, **TAPP-M-An** (M = Mn, Cu) at E_x = 330 nm, E_m = 369 nm. d) Calculated HOMO and LUMO for the model molecule **TAPP-Cu-An**. e) Contour plot of spin population of **TAPP-Cu-An**.

that **TAPP-An** has higher catalytic efficiency than **TAPP-Cu-An** in the initial catalytic process. Experimental results showed that when using a mixture of 1a and 2c as reactants, **TAPP-Cu-An** exhibited unexpectedly high catalytic performance. Based on the computational results, we hypothesize that this may be because, in the presence of both 1a and 2c, 2c also has high adsorption energy with the Cu atom, significantly competing with 1a (Figure S53c,e,g,i, Supporting Information). This forces more 1a to participate in the first process of the catalysis, enhancing the catalytic efficiency. In subsequent catalytic steps, the significant spin population on the Cu atom (Figure 5e) allows the adsorbed 2c to also participate in the second catalytic process, further increasing the catalytic efficiency. Therefore, **TAPP-Cu-An** showed the best catalytic performance in one step tandem reaction. The main reason is that the synergistic catalysis of TAPP-Cu and An can achieve a reasonable directional adsorption of the two substrates, improve the yield of 2a intermediates in process 1, and the high catalytic activity of Cu metal site accelerates the intramolecular dehydrogenation coupling reaction in process 2.[13]

Therefore, based on the above experimental data, theoretical calculation results, and previous reports,[4,13,41,42] a plausible reaction mechanism was proposed (**Figure 6**). In the tandem catalytic reaction, O_2 is first activated to form $^1O_2$ by both TAPP-Cu and An units.[43,44] Then, $^1O_2$ oxidizes the substrates/intermediates adsorbed at the TAPP-Cu and An into intermediates/tagret products, while itself accepting two photogenerated electrons and two H^+ (removed from the oxidized substrate) to form H_2O_2.[42] The generated H_2O_2 is immediately catalyzed by **TAPP-Cu-An** to form •OH, which continues to participate in the catalytic oxidation reaction and eventually forms H_2O.

In order to verify our conjecture and exclude the influence of H_2O_2, we first performed iodometry for color development of the reaction solution immediately and determined the H_2O_2 content in it by ultraviolet absorption spectrometry. No UV absorption peak of H_2O_2 was found in the test results (Figure S44a, Supporting Information). After that, **TAPP-An** and **TAPP-Cu-An** were immersed in H_2O_2 iodometric chromogenic solution respectively,

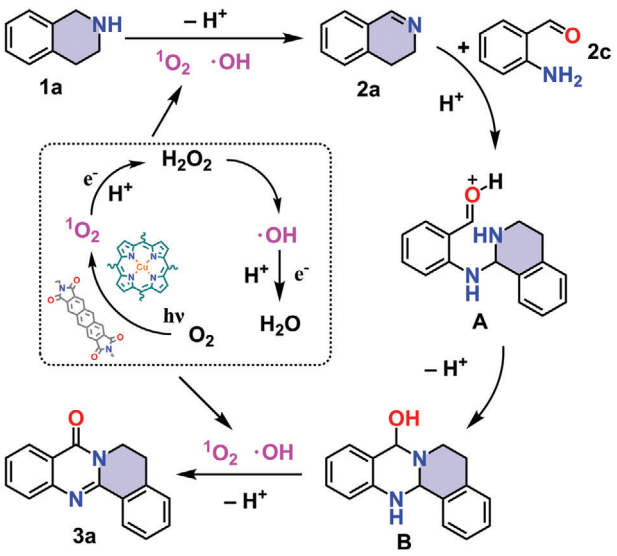

Figure 6. The probable mechanism of the dehydrogenative cross-coupling reaction between 1a and 2c.

and the change of H_2O_2 content was detected by UV absorption spectrum. The results show that both **TAPP-Cu-An** and **TAPP-An** can accelerate the decomposition of H_2O_2, and the rate of **TAPP-Cu-An** is the fastest (Figure S44b,c,d, Supporting Information). This confirms our conjecture about the reaction mechanism, that is the reaction $^1O_2$ is first converted to H_2O_2, and then H_2O_2 is decomposed and produced •OH. Therefore, we believe that most of the generated H_2O_2 is decomposed in the reaction and has no effect on the catalytic reaction.

3. Conclusion

In summary, we purposefully developed two photosensitive and stable COFs, which act as unprecedented heterogeneous tandem catalysts to complete the dehydrogenative cross-coupling reaction of 1,2,3,4-tetrahydroisoquinoline and 2-aminobenzaldehyde in a mild and energy-efficient manner in a short time, and thus to achieve an efficient photosynthesis of 4-quinazolinone drug molecules. Especially the best-performing **TAPP-Cu-An**, with excellent photogenerated charge separation and transport and efficient An-Cu co-catalysis, allows the photosynthesis of 4-quinazolinones at high conversion (>99%) and selectivity (>99%) within 6 h and easily achieves gram-scale reactions. Moreover, the corresponding catalytic reaction processes, mechanisms, and performance enhancement were confirmed by single/combined COF catalysts-induced one-step/stepwise photoconversion experiments incorporated with theoretical calculations. This work confirms for the first time the important application of COF catalysts in the synthesis of 4-quinazolinones, in which the strategy of synergistic tandem catalysis of pre-designed active components can be further used to facilitate more important organic synthesis reactions involving different catalytic processes.

4. Experimental Section

Synthesis of ***TAPP-An***: 5,10,15,20-Tetrakis(4-aminophenyl) porphyrin (46.2 mg, 0.068 mmol, TAPP), 1*H*,3*H*-Anthra[2,3-*c*:6,7-*c'*]difuran-1,3,7,9-tetrone (43.2 mg, 0.136 mmol, An), anhydrous zinc chloride (228 mg, 1.66 mmol) and sodium chloride (74.4 mg, 1.27 mmol) were ground to a fine powder in a mortar under inert atmosphere and transferred into a 20 cm long spherical quartz tube. The quartz tube was evacuated (<1000 mbar) for 10 min, then flame sealed and heated to 250 °C for 72 h in a tube furnace or a muffle furnace. The quartz tube was cooled to room temperature. The crude product was ground in a mortar and washed with 1 M HCl, water, and THF. The solvent exchange was carried out by Soxhlet extraction with methanol overnight. The solvent was removed via supercritical CO_2 drying to afford **TAPP-An** as a black powder.

Synthesis of ***TAPP-Mn-An***: 5,10,15,20-Tetrakis(4-aminophenyl) porphyrin-Mn (25.5 mg, 0.035 mmol, TAPP-Mn), 1*H*,3*H*-Anthra[2,3-*c*:6,7-*c'*]difuran-1,3,7,9-tetrone (21.6 mg, 0.068 mmol, An), anhydrous zinc chloride (114 mg, 0.83 mmol) and sodium chloride (12.4 mg, 0.21 mmol) were ground to a fine powder in a mortar under inert atmosphere and transferred into a 20 cm long spherical quartz tube. The quartz tube was evacuated (<1000 mbar) for 10 min, then flame sealed and heated to 250 °C for 72 h in a tube furnace or a muffle furnace. The quartz tube was cooled to room temperature and then opened. The crude product was ground in a mortar and washed with 1 M HCl, water, and THF. The solvent exchange was carried out by Soxhlet extraction with methanol overnight. The solvent was removed via supercritical CO_2 drying to afford **TAPP-Mn-An** as a black powder.

Synthesis of ***TAPP-Cu-An***: 5,10,15,20-Tetrakis(4-aminophenyl) porphyrin-Cu (25.2 mg, 0.034 mmol, TAPP-Cu), 1*H*,3*H*-Anthra[2,3-*c*:6,7-*c'*]difuran-1,3,7,9-tetrone (21.6 mg, 0.068 mmol, An), anhydrous zinc chloride (114 mg, 0.83 mmol) and sodium chloride (6.2 mg, 0.11 mmol) were ground to a fine powder in a mortar under inert atmosphere and transferred into a 20 cm long spherical quartz tube. The quartz tube was evacuated (<1000 mbar) for 10 min, then flame sealed and heated to 250 °C for 72 h in a tube furnace or a muffle furnace. The quartz tube was cooled to room temperature and then opened. The crude product was ground in a mortar and washed with 1 M HCl, water, and THF. The solvent exchange was carried out by Soxhlet extraction with methanol overnight. The solvent was removed via supercritical CO_2 drying to afford **TAPP-Cu-An** as a black powder.

Supporting Information

Supporting Information is available from the Wiley Online Library or from the author.

Acknowledgements

This work was supported by the National Key R&D Program of China (2024YFA1510700, 2023YFA1507201 and 2023YFA1507204), the National Natural Science Foundation of China (22271104, 22225109, 22071109 and 22201046), the Young Top Talents of Pearl River Talent Program of Guangdong Province (2021QN02L617) and the Guangdong Basic and Applied Basic Research Foundation (2023B1515120060 and 2023A1515030097).

Conflict of Interest

The authors declare no conflict of interest.

Author Contributions

Y.C and S.-N.S contributed equally to this work. Y.-Q.L, J.L, and Y.C conceived and designed the idea. Y.C synthesized the COF catalysts. Y.C, S.-N.S, X.-H.C, M.-L.C, and Q.N conducted the characterizations and designed the catalytic reaction-related experiments. Y.-Q.L, J.L, J.-M.L, S.L.L, S.-N.S and Y.C. discussed the result and prepared the manuscript. All the authors reviewed and contributed to this paper.

Data Availability Statement

The data that support the findings of this study are available in the supplementary material of this article.

Keywords

covalent-organic frameworks, pharmaceutical synthesis, photocatalyst

Received: September 11, 2024
Revised: December 11, 2024
Published online:

[1] C. Pratley, S. Fenner, J. A. Murphy, *Chem. Rev.* **2022**, *122*, 8181.
[2] S. K. Sinha, S. Guin, S. Guin, J. P. Biswas, S. Porey, D. Maiti, *Chem. Rev.* **2022**, *122*, 5682.

[3] J. Chen, K. Natte, A. Spannenberg, H. Neumann, P. Langer, M. Beller, X.-F. Wu, *Angew. Chem., Int. Ed.* **2014**, *53*, 7579.
[4] D. Jing, C. Lu, Z. Chen, S. Jin, L. Xie, Z. Meng, Z. Su, K. Zheng, *Angew. Chem., Int. Ed.* **2019**, *58*, 14666.
[5] J.-H. An, Y.-H. Wang, Z.-X. Zhang, Z.-T. Zhao, J. Zhang, F. Wang, *Angew. Chem., Int. Ed.* **2018**, *57*, 12308.
[6] A. Shatskiy, G. R. Alvey, M. D. Kärkäs, *Chem.* **2022**, *8*, 12.
[7] J. Li, Z.-B. Wang, Y. Xu, X.-C. Lu, S.-R. Zhu, L. Liu, *Chem. Commun.* **2019**, *55*, 12072.
[8] E. P. Beaumier, A. A. Ott, X. L. Wen, Z. W. Davis-Gilbert, T. A. Wheeler, J. J. Topczewski, J. D. Goodpaster, I. A. Tonks, *Chem. Sci.* **2020**, *11*, 7204.
[9] Q.-Q. Cheng, Y.-M. Deng, M. Lankelma, M. P. Doyle, *Chem. Soc. Rev.* **2017**, *46*, 5425.
[10] R. Remy, C. G. Bochet, *Chem. Rev.* **2016**, *116*, 9816.
[11] L. E. Zetzsche, J. A. Yazarians, S. Chakrabarty, M. E. Hinze, L. A. M. Murray, A. L. Lukowski, L. A. Joyce, A. R. H. Narayan, *Nature.* **2022**, *603*, 79.
[12] C. Lu, Z. Su, D. Jing, S. Jin, L. Xie, L. Li, K. Zheng, *Org. Lett.* **2019**, *21*, 1438.
[13] T. T. Nguyen, K. X. Nguyen, P. H. Pham, D. Ly, D. K. Nguyen, K. D. Nguyen, T. T. Nguyen, N. T. S. Phan, *Org. Biomol. Chem.* **2021**, *19*, 4726.
[14] F. Xie, Q.-H. Chen, R. Xie, H.-F. Jiang, M. Zhang, *ACS Catal.* **2018**, *8*, 5869.
[15] C. S. Diercks, O. M. Yaghi, *Science.* **2017**, *355*, eaal1585.
[16] J.-Q. Dong, X. Han, Y. Liu, H.-Y. Li, Y. Cui, *Angew. Chem., Int. Ed.* **2020**, *59*, 13722.
[17] S.-Y. Ding, W. Wang, *Chem. Soc. Rev.* **2013**, *42*, 548.
[18] B. Wang, R.-B. Lin, Z. Zhang, S. Xiang, B. Chen, *J. Am. Chem. Soc.* **2020**, *142*, 14399.
[19] N. Huang, X. Chen, R. Krishna, D. Jiang, *Angew. Chem., Int. Ed.* **2015**, *54*, 2986.
[20] H. Fan, A. Mundstock, A. Feldhoff, A. Knebel, J. Gu, H. Meng, J. Caro, *J. Am. Chem. Soc.* **2018**, *140*, 10094.
[21] R. Chen, Y. Wang, Y. Ma, A. Mal, X.-Y. Gao, L. Gao, L. Qiao, X.-B. Li, L.-Z. Wu, C. Wang, *Nat. Commun.* **2021**, *12*, 1354.
[22] M. Lu, M. Zhang, C.-G. Liu, J. Liu, L.-J. Shang, M. Wang, J.-N. Chang, S.-L. Li, Y.-Q. Lan, *Angew. Chem., Int. Ed.* **2021**, *60*, 4864.
[23] N. Huang, K. H. Lee, Y. Yue, X. Xu, S. Irle, Q. Jiang, D. Jiang, *Angew. Chem., Int. Ed.* **2020**, *59*, 16587.
[24] Y. Lin, H. Cui, C. Liu, R. Li, S. Wang, G. Qu, Z. Wei, Y. Yang, Y. Wang, Z. Tang, H. Li, H. Zhang, C. Zhi, H. Lv, *Angew. Chem., Int. Ed.* **2023**, *62*, 202218745.
[25] W. Wang, V. S. Kale, Z. Cao, Y. Lei, S. Kandambeth, G. Zou, Y. Zhu, E. Abouhamad, O. Shekhah, L. Cavallo, M. Eddaoudi, H. N. Alshareef, *Adv. Mater.* **2021**, *33*, 2103617.
[26] S. Zheng, D. Shi, D. Yan, Q. Wang, T. Sun, T. Ma, L. Li, D. He, Z. Tao, J. Chen, *Angew. Chem., Int. Ed.* **2022**, *61*, 202117511.
[27] M. Traxler, S. Gisbertz, P. Pachfule, J. Schmidt, J. Roeser, S. Reischauer, J. Rabeah, B. Pieber, A. Thomas, *Angew. Chem., Int. Ed.* **2022**, *61*, 202117738.
[28] Y. Fan, D. W. Kang, S. Labalme, J. Li, W. Lin, *Angew. Chem., Int. Ed.* **2023**, *62*, 202218908.
[29] Q. Fang, S. Gu, J. Zheng, Z. Zhuang, S. Qiu, Y. Yan, *Angew. Chem., Int. Ed.* **2014**, *53*, 2878.
[30] M. Bhadra, S. Kandambeth, M. K. Sahoo, M. Addicoat, E. Balaraman, R. Banerjee, *J. Am. Chem. Soc.* **2019**, *141*, 6152.
[31] A. López-Magano, S. Daliran, A. R. Oveisi, R. Mas-Ballesté, A. Dhakshinamoorthy, J. Alemán, H. Garcia, R. Luque, *Adv. Mater.* **2023**, *35*, 2209475.
[32] T.-Y. Zhou, S.-Q. Xu, Q. Wen, Z.-F. Pang, X. Zhao, *J. Am. Chem. Soc.* **2014**, *136*, 15885.
[33] Q. Lu, Y. Ma, H. Li, X. Guan, Y. Yusran, M. Xue, Q. Fang, Y. Yan, S. Qiu, V. Valtchev, *Angew. Chem., Int. Ed.* **2018**, *57*, 6042.
[34] S. Liu, M. Wang, T. Qian, H. Ji, J. Liu, C. Yan, *Nat. Commun.* **2019**, *10*, 3898.
[35] P. Das, G. Chakraborty, J. Roeser, S. Vogl, J. Rabeah, A. Thomas, *J. Am. Chem. Soc.* **2023**, *145*, 2975.
[36] R. Chen, D. Wang, W. Hao, F. Shao, Y. Zhao, *Chem. Commun.* **2021**, *57*, 5794.
[37] Y.-R. Wang, H.-M. Ding, X.-Y. Ma, M. Liu, Y.-L. Yang, Y. Chen, S.-L. Li, Y.-Q. Lan, *Angew. Chem., Int. Ed.* **2022**, *61*, 202114648.
[38] J. Maschita, T. Banerjee, G. Savasci, F. Haase, C. Ochsenfeld, B. V. Lotsch, *Angew. Chem., Int. Ed.* **2020**, *59*, 15750.
[39] R. Gao, X. Mei, D. Yan, R. Liang, M. Wei, *Nat. Commun.* **2018**, *9*, 2798.
[40] H. Xiao, J. Tahir-Kheli, W. A. Goddard, *J. Phys. Chem. Lett.* **2011**, *2*, 212.
[41] B. Sun, P.-Y. Huang, Z.-Y. Yan, X.-Y. Shi, X.-L. Tang, J. Yang, C. Jin, *Org. Lett.* **2021**, *23*, 1026.
[42] X.-K. Zeng, T.-Y. Wang, Z.-Y. Wang, M. Tebyetekerwa, Y. Liu, Z.-Y. Liu, G. Wang, A. A. Wibowo, G. Pierens, Q.-F. Gu, X.-W. Zhang, *ACS Catal.* **2024**, *14*, 9955.
[43] H.-G. Jeong, M.-S. Choi, *Isr. J. Chem.* **2016**, *56*, 110.
[44] H. Lai, J. Yan, S. Liu, Q. Yang, F. Xing, P. Xiao, *Angew. Chem., Int. Ed.* **2020**, *59*, 10431.